Advanced Steel Construction – Vol. 18 No. 4 (2022) 773–782
DOI:10.18057/IJASC.2022.18.4.5

QUANTITATIVE EVALUATION OF EFFECT OF VARIOUS SPAN-TO-DEPTH RATIOS ON THE COLLAPSE PERFORMANCE OF PLANAR STEEL FRAMES

Zheng Tan [1], Wei-Hui Zhong [1, 2, *], Yu-Hui Zheng [1], Shi-Chao Duan [1], Bao Meng [1] and Cheng Jiang [1]

[1] *School of Civil Engineering, Xi'an University of Architecture and Technology, Xi'an 710055, China*
[2] *Key Laboratory of Structural Engineering and Earthquake Resistance, Ministry of Education, Xi'an University of Architecture and Technology, Xi'an 710055, China*
** (Corresponding author: E-mail: zhongweihui1980@163.com)*

ABSTRACT

After the removal of a column caused by the unexpected extreme loading of the building structure, the remaining structure mainly relies on the double-span beams connected with the failed column to mitigate the progressive collapse, therefore, the span-to-depth ratios of the double-span beams has significant effects on the internal force redistribution among each story and the development of the anti-collapse mechanisms of the multi-story planar frames. To investigate the effect of span-to-depth ratios on the progressive collapse performance of steel frames, the collapse analysis of three-story steel frame models with various beam depths and beam spans was numerically studied. Firstly, the correctness of the numerical modeling method was verified by the collapse test results of a two-story sub-frame. Then, the refined modeling methods were applied to the analysis of progressive collapse performance of steel frames with various span-to-depth ratios. The load response, load distribution, deformation characteristic and load-resisting mechanisms of models are investigated in detail. The results showed that the resistances provided by flexural mechanism and catenary mechanism are mainly determined by span-to depth ratios and beam span, respectively. Through the principle of energy conservation, the different resistant contribution coefficients of each story are quantitatively obtained, and corresponding empirical formulas were proposed, which can be used as a reference for resistance evaluation before the design of structural anti-collapse.

ARTICLE HISTORY

Received: 8 May 2022
Revised: 16 May 2022
Accepted: 17 May 2022

KEYWORDS

Progressive collapse;
Numerical simulation;
Vierendeel action;
Span-to-depth ratio;
Quantitative assessment

1. Introduction

With the rapid tide of development to large-scale and complex nature of modern architectures, especially with the frequent occurrence of natural and man-made disasters, building structures are alarmingly prone to a progressive collapse. Therefore, ensuring the structural overall stability under unexpected extreme loading has become one of the hot research problems in structural engineering [1-2]. The progressive collapse behavior of frame structures has been globally explored by researchers in the past decade. At present, performing a continuous path analysis of the residual load followed by that of the original structure is one of the most commonly applied methods to ensure the structural collapse resistance. Due to the financial and laboratory limitations, the collapse test of frame structures mostly uses a single-story beam-column assembly as the research object, and systematically studies important parameters such as the connection type [3-5], boundary condition [6-7], floor combination action [8], and double-span beams with unequal span [9-11]. These valuable studies preliminarily reveal the development law of the resistance mechanisms of beam members in the process of collapse. However, because the progressive collapse of buildings is a relatively complex mechanical behavior [12-13], it is unreasonable to analyze the structural load-bearing capacity based on the structural scale of a single-story frame [14-15], so as to provide design reference for building structures.

Comparison of the collapse resistance between single-story frames and multi-story frames revealed that the collapse resistance between two different structural scale models is not based on the number of stories because of the existence of Vierendeel action (VA) [16-18]. Qian et al. [19-20], Tsito et al. [21] and Zhong et al. [22] have conducted quasi-static collapse tests, and subsequently, compared and analyzed in detail the influence of connection type, failure column position, and other parameters on the structural performance. Their results show that the connection types and failure column position exhibit a considerable influence on the exertion of catenary action. However, considering the high cost, only the sub-frame in the direct influence area was considered while fabricating the experimental specimens. The extended beams is generally connected to the horizontal restraint device to consider the tie effect resulting from the peripheral frames. However, this simplification of boundary constraint for each story is not consistent with the actual boundary constraint [23-24], which may result in an miscalculation of structural resistant performance. In addition, the above experimental objects were all scaled owing to high cost, however, the scale effect may has an unneglected effect on the structural collapse behavior. Therefore, the collapse research objects should focus on the overall frames with considering the effect of VA, rather than single-story beam-column assemblies.

After a local failure of the structure caused by a sudden load, the vertical load was resisted by redistributing the shear force at beam ends and axial force in the double-span beams [25-26]. Therefore, the span-to-depth ratio of double-span beams affects the development of different resistance mechanisms. At present, research on the anti-collapse behavior of planar frames with various span-to-depth ratios is very limited. The author previously studied the effect of different beam linear stiffness on the collapse behavior of single-story frames [27]. However, there may be a considerable difference between the collapse behavior of components in the overall structure and the structural collapse performance of single-story frame (single component) under column removal scenario.

From the above review, the current researches outcomes mainly focus on the single-story frames under component level, whereas the research on the structural performance of overall planar frames is still scarce. The overall performance analysis of the internal force transfer between beam members and the development law of resistance mechanisms needs to be further studied, especially for the influence of double-span beams with various span-to-depth ratios on the structural performance. In view of the high cost of conducting the collapse tests on overall planar steel frames with various span-to-depth ratios, it is necessary to quantitatively evaluate the effect of the span-to-depth ratios on the collapse behavior of planar frames using the numerical analysis method. Therefore, in this paper, the finite element model (FEM) was first verified by comparing the test results of the two-story sub-frame proposed by Qian et al. [19]. Then, based on the refined model using shell element, a detailed numerical simulation of the resistant collapse performance of three-story planar steel frames with various span-to-depth ratios was investigated in detail, and the different resistant contribution coefficients of different stories of multi-story steel frames were quantitatively separated, which can serve as a reference for collapse resistance evaluation prior to designing the multi-story planar steel frames to mitigate progressive collapse.

2. Numerical verification

2.1. Design of multi-story planar steel frames

Three-story, four-span planar steel frames with various span-to-depth ratios were designed in accordance with the steel structure design standard GB50017-2017 [28]. The dead load (*DL*) used in the design of structures is 5.0 kN/m^2 and the live load (*LL*) is 2.5 kN/m^2. The geometric parameters of the planar frames are as follows: the beam span and story height of the frame structure are 6000 and 3000 mm, respectively. Through structural design and analysis, the column and beam sections with H450 × 300 × 11 × 18 (mm), H400 × 200 × 8 × 13 (mm) were selected, respectively. The reduced beam section (RBS) connection was adopts in the frames, and the dimension of connection is shown in Fig. 1. The RBS connection exhibits good ductility, which was favourable to the development of vertical displacement in the

catenary mechanism stage through moving plastic hinge away from the beam ends [29]. The design of the weakening parameters of the beam flange were calculated by the ANSI/AISC 358 standard [30], as sated in Eqs. (1)~(4). The specific dimension of the weakening parameters of RBS cut are shown in Fig. 1, in which *a*, *b* and *c* are 120 mm, 300 mm and 40 mm, respectively.

$$0.5b_f \le a \le 0.75b_f \tag{1}$$

$$0.65h \le b \le 0.85h \tag{2}$$

$$0.1b_f \le c \le 0.25b_f \tag{3}$$

$$R = \frac{4c^2 + b^2}{8c} \tag{4}$$

where b_f is flange width of beam; h is the beam depth.

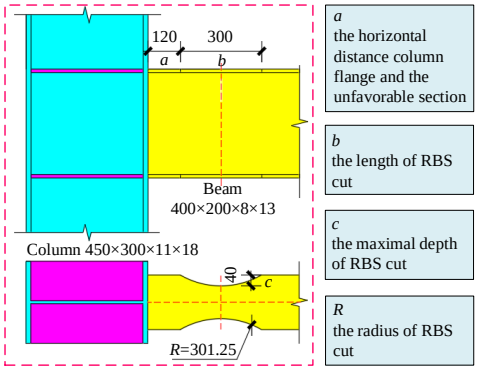

Fig. 1 Dimension of RBS connection (unit: mm)

2.2. Modeling of FEM

2.2.1. Design of structural parameters

Regarding the span-to-depth ratio of the double-span beams connected to the failed column as the research parameter, changing the beam span or beam depth of the double-span beams, corresponding to case (1) and case (2). The multi-story planar frame with beam depth of 400mm and span of 6000mm as the standard model. Models with various span-to-depth ratios in the range of 10~30 were selected. In two different cases, the structural parameters include beam span (*L*), *h*, span-to-depth ratio (*L*/*h*) and beam linear stiffness (*k*), as summarized in Table 1.

Table 1
Design of structural parameters

	Model	*L*/mm	*h*/mm	*L*/*h*	*k*/(kN·m)
Case (1)	RBS-S1	4000	400	10	118270
	RBS-S2	4800		12	98558
	RBS-S3	6000		15	78847
	RBS-S4	8000		20	59135
	RBS-S5	12000		30	39423
Case (2)	RBS-D1	6000	200	30	16839
	RBS-D2		300	20	41498
	RBS-D3		400	15	78847
	RBS-D4		500	12	130257
	RBS-D5		600	10	197105

Note: "S" and "D" presented span and depth of beam; Model RBS-S3 and model RBS-D3 were the same model; $k=EI/L$, E is the elastic modulus of steel, I is section moment of inertia of the steel beam.

2.2.2. Material model

In order to make the calculation results meet the requirements of static analysis, the kinetic energy of the model was less than 10% of the total internal energy [31]. Q345 grade steel (yield strength f_y=345MPa, tensile strength f_u=518MPa) was adopted, respectively. The elastic modulus E Poisson's ratio were 2.06×10^5MPa and 0.3, respectively. The multilinear constitutive model [11] was used for the stress-strain relationship of steel. The ductile metal failure criterion was employed to reconstruct the fracture process of models under large deformation stage and the equivalent plastic damage strain of steel ($\bar{\varepsilon}_0^{pl}$) [32] can be calculated according to Eqs. (5)~(8) .

$$\frac{-pl}{\varepsilon_0} = \begin{cases} \infty, & \eta \le -1/3 \\ C_1/(1+3\eta), & -1/3 \le \eta \le 0 \\ C_1 + 9(C_2 - C_1)\eta^2, & 0 \le \eta \le \eta_0 \\ C_2/3\eta, & \eta_0 \le \eta \end{cases} \tag{5}$$

Here, η is the triaxial stress; C_1 and C_2 are the $\bar{\varepsilon}_0^{pl}$ of steel under pure shear and uniaxial tension, respectively, and can be determined by Eqs. (6)~(8).

$$C_2 = -\ln(1 - A_R) \tag{6}$$

$$C_1 = C_2(\sqrt{3}/2)^{1/n} \tag{7}$$

$$\sigma = K(\varepsilon)^n \tag{8}$$

where A_R is the reduced cross-sectional area; K and n are the hardening parameters of steel.

2.2.3. Boundary conditions and meshing

All beam and column members adopt S4R shell element. The connection between beam and column adopts the "Tie" command. Because the model size and boundary constraints are completely symmetrical, in order to save the calculation cost, only 1/2 model was established for numerical simulation analysis. The established FEM is illustrated in Fig. 2. For the failed and side columns, it is necessary to limit theirs out-of-plane displacement. The loading process adopts displacement control with a smooth analysis step. The six degrees of freedom of the bottom of the two side columns were constrained. For the stress concentration area of beam-to-column connections, dense grid elements with 10 mm was employed. For other beam and column members, 100mm was selected for other parts considering the calculation efficiency.

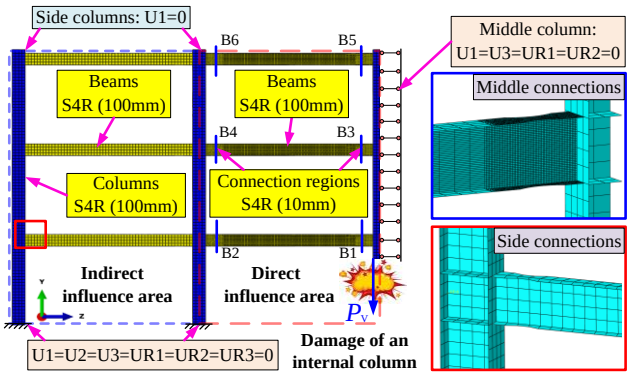

Fig. 2 Numerical modeling information of FEM

2.3. Verification of modeling methods

Before conducting the simulation numerical study, the modeling methods of the FEM was validated by the experimental results by Qian et al. [19]. A 1/2 scaled two-story steel frame with RBS connection was tested subjected to the loss of a middle column. Fig. 3 illustrated the test setup and dimensions of the RBS connections. The beam span and story height of the specimen were 3000 and 1500 mm, the length of the extended beam was 655 mm. H150 × 150 × 7 × 10 (mm) and H200 × 100 × 5.5 × 8 (mm) sections were employed to the beams and columns, respectively. The measured material properties of the frame are summarized in Table 2. The bottom of the side columns are connected with hinged connectors, and the extended beams were connected with the A-frame. At the top of the failed column, the vertical load applied by the jack was applied to simulate the removal process of the internal column until the specimen was completely destroyed. During the loading process, the

specimen was restrained by the lateral steel column to prevent lateral instability, and two-point loads were applied to the tops of the side columns. The detail of the experimental test, please refer to Qian et al. [19].

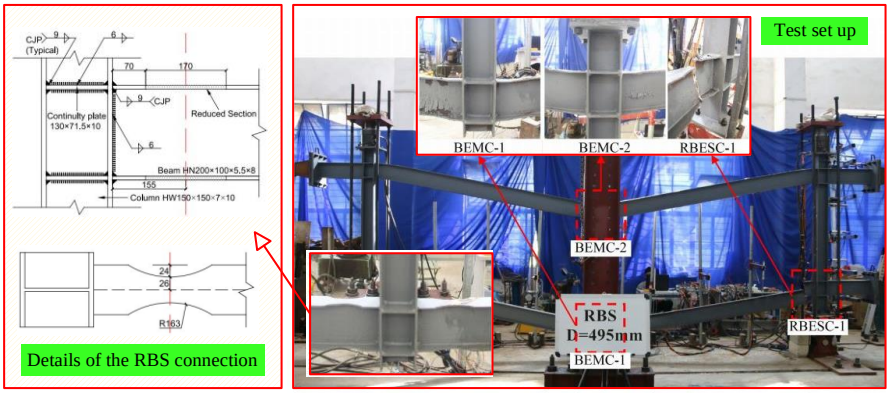

Fig. 3 Collapse test of two-story steel frame with RBS connection [19] (dimension units: mm)

Table 2
Material properties of the steel [19].

Members	Yield strength/ MPa	Ultimate strength/ MPa	Elastic modulus / GPa	Elongation/ %
Beam flange	310	420	315	12.0
Beam web	320	430	340	13.5
Column	300	410	430	14.0
Column web	295	375	265	13.0

The FEM corresponding the two-story sub-frame was established, as shown in Fig. 4. Four axial connectors were employed at the outreached beams to consider the tie effect provided by the A-frame. Axial connectors at the first and second stories with the axial stifnesses of 39.2 and 31.0 kN/mm, while the gaps were 0.7 and 0.9 mm, respectively.

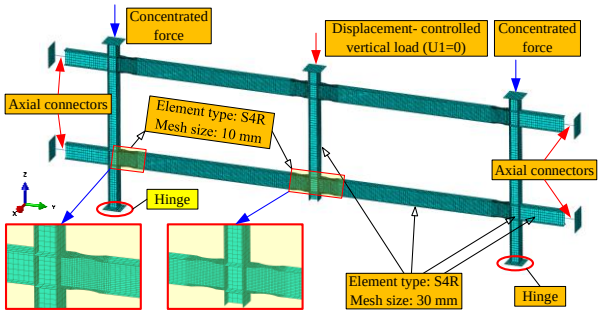

Fig. 4 FEM of the two-story sub-frame

The comparison between the numerical results predicted by FEM and the test results of the two-story sub-frame is presented in Fig. 5. It can be observed that the load–displacement curve from the results of the experimental sub-frame and FEM were in complete agreement, as illustrated in Fig. 5(a). The initial stiffness and plastic load are almost the same, and the error between the ultimate load and corresponding displacement (466 mm, 389 kN) obtained by numerical simulation and the experimental value (468 mm, 407 kN) is less than 5%, which shows that the simulation results have enough accuracy. The comparison of the failure modes predicted by the FEM and test results is shown in Fig. 5(b). It shows that the modeling methods can accurately forecast the fracture location and reproduce post fracture development path of sub-frame. Therefore, the numerical modeling methods can be employed to explore the influence of the span-to-depth ratio on the collapse-resistant performance of planar frames.

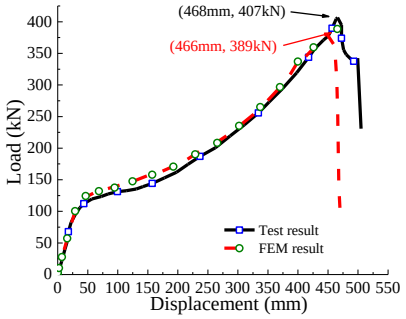

(a) The load-displacement curve

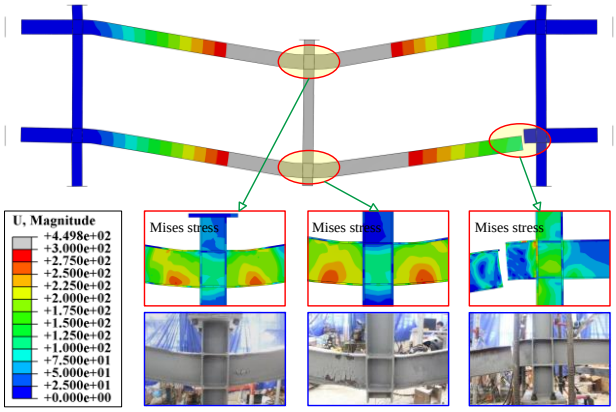

(b) Failure mode

Fig. 5 Comparison of the results of the two-story sub-frame from the test [19] and FEM

3. Analysis of span-to-depth ratio on structural collapse performance

3.1. Parameter normalization

In order to facilitate comparative analysis, the vertical displacement of the failed column, the axial force, the bending moment and the vertical load of the failed column are normalized through appropriate indicators, that is, the resulting parameters are dimensionless. The theoretical values of the corresponding index parameters are illustrated in Table 3. The vertical displacement of the failed column can be normalized by the clear span (l) of the double-span beams to characterize the relative vertical deformation of the double-span beams; The axial force of the midspan section can be normalized by the axial tensile yield force (N_p) of the most unfavorable section, with an aim to characterize the development degree of the axial force; The bending moment of the most unfavorable section can be normalized by the plastic bending capacity (m_{p+} and m_{p-}) of the most unfavorable section to characterize the degree of plastic development of the most unfavorable section, which can be calculated according to Eqs. (9) and (10).

$$N_p = f_y A \tag{9}$$

$$m_p = W_p f_y \tag{10}$$

where A is the cross section area of the most unfavorable section; W_p is the plastic section modulus of the most unfavorable section.

The vertical load was normalized by the theoretical plastic load (P_p) to characterize the structural collapse resistance. The plastic load of three-story steel frame can be calculated by plastic analysis method (see Fig. 6), which was calculated by Eq. (11).

$$P_p v = 2\theta(M_{p+} + M_{p-}), \quad \theta = v/l \tag{11}$$

The bending moments at beam ends (M_p) and most unfavorable section (m_p) can be converted through by Eq. (12).

$$\frac{m_{p-}}{M_{p-}} = \frac{m_{p+}}{M_{p+}} = (l - a - b/2)/l \tag{12}$$

where a and b were defined shown in Fig. 1.

Finally, combining Eqs. (11) and (12), the plastic load of the three-story steel frame can be calculated as follows:

$$P_p = \frac{6(m_{p+} + m_{p-})}{l - a - b/2} \tag{13}$$

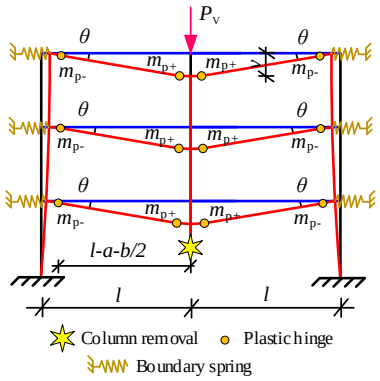

Fig. 6 Plastic analysis method for calculation of the plastic load of multi-story planar frame

Table 3
Theoretical value of structural parameters

	Model	P_p/kN	N_p/kN	m_{p+}/(kN·m)	m_{p-}/(kN·m)
Case (1)	RBS-S1	1116	2109	305	-305
	RBS-S2	897			
	RBS-S3	693			
	RBS-S4	503			
	RBS-S5	324			
Case (2)	RBS-D1	277	1557	122	-122
	RBS-D2	459		206	-206
	RBS-D3	693		305	-305
	RBS-D4	948		417	-417
	RBS-D5	1234		543	-543

3.2. Load response analysis

The load response curves of two models with various span-to-depth ratios are illustrated in Fig. 7, including the static load-displacement, dimensionless load-displacement, and pseudo static load-displacement curves. As shown in Fig. 7(a1) and (b1), the plastic load of each model increases with the increase in the *L*/*h*. Except for model rbs-d1, the final failure displacement of other models is approximately 1/5th of the span, which is close to the failure limit of frame structure in the code (1/5th of beam span [2]). Many experimental studies on the collapse of single-story frames [3,5] show that the failure displacement of substructures is far greater than the failure limit specified in the code. The major reasons for the significant difference in the conclusions of structural failure displacement between the two different scale models are the following: (1) the difference of boundary constraints (the main reason) and (2) the scale effect of the substructure (the secondary reason). This further shows that the resistance of single-story frame cannot reflect the mechanical properties of a multi-story frame structure under collapse conditions. In addition, the later bearing capacity of different span models shows a relatively gentle development trend, and its value is equivalent to the plastic bearing capacity. For different beam height models, the later bearing capacity of the model with larger beam depth shows a downward trend, while the later bearing capacity of the model with smaller beam height shows a rising trend.

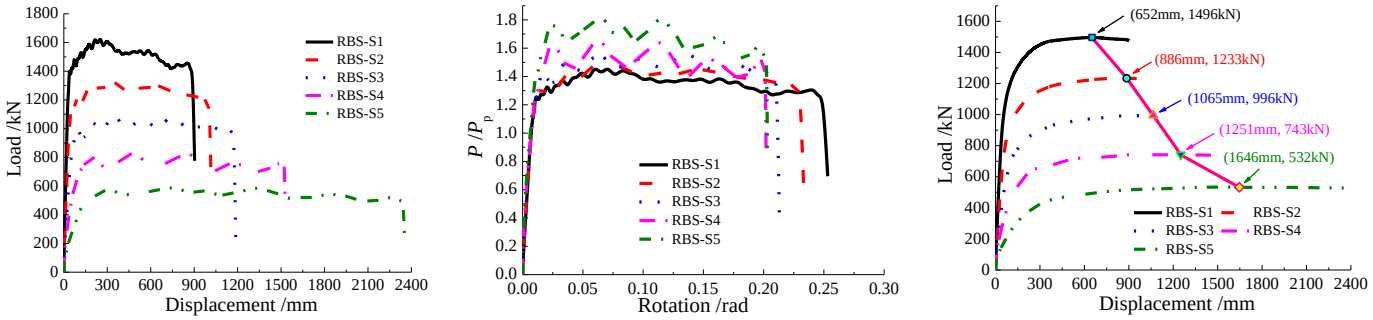

(a1) Load-displacement curve (a2) Load-displacement curve (Dimensionless) (a3) Pseudo static load-displacement curve

(a) Case (1)

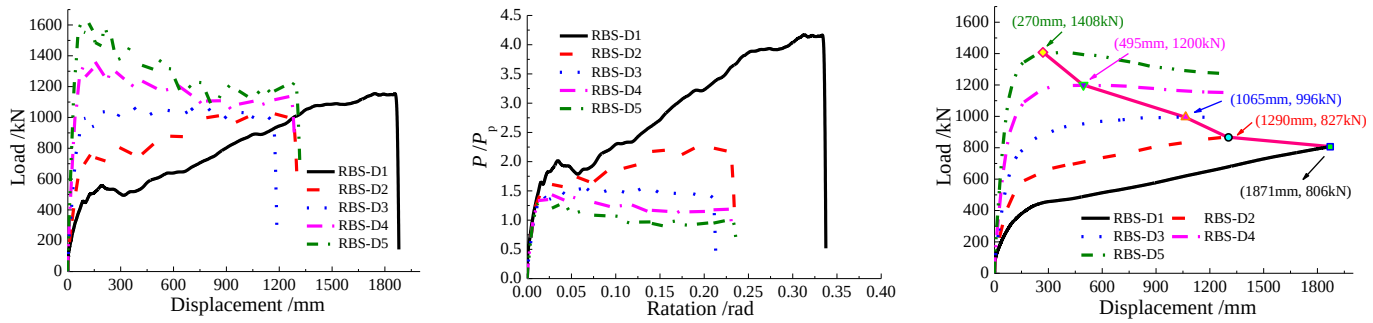

(b1) Load-displacement curve (b2) Load-displacement curve (Dimensionless) (b3) Pseudo static load-displacement curve

(b) Case (2)

Fig. 7 Comparison of load response curves of models under different cases

The dimensionless load displacement curves corresponding to each model are shown in Fig. 7(a2) and (b2). With the increase in the *L*/*h*, the P/P_p value of each model decreases in turn, and the P/P_p value of model RBS-D1 finally reaches 4, indicating that the catenary mechanism of this model has been brought into full play compared with other models. This is because the tie demand of the frame structure in the directly affected area for the surrounding frames is related to the beam-column linear stiffness ratio, so the same peripheral restraint frame exhibits a stronger tie effect for the connections with relatively small beam-column linear stiffness, which was conducive to the effective play of the catenary action in the later stage of the lower beams.

Based on the static load displacement curve, the pseudo static load displacement curve of each model can be obtained through the energy conversion principle [33]. As shown in Fig. 7(a3) and (b3), the pseudo static load of each model increases with the decrease in the *L*/*h*, but the corresponding displacement decreases, indicating that under the action of dynamic load, the model with smaller *L*/*h* of double-span beams has a better bearing capacity, but it was not conducive to the structural vertical displacement in the column removal scenario.

3.3. Internal force development

3.3.1. Axial force development

The axial force development of models with various span-to-depth ratios is shown in Fig. 8. The axial tension is mainly concentrated in the bottom story ($0.30N_p$~$1.00N_p$), while the double-span beams of the top story is mainly in the compressed state (-$0.15N_p$~0) during the process resisting vertical load, and the middle story exhibits a continuously developing axial tension ($0.10N_p$~$0.25N_p$). All the models exhibit the obvious characteristics of a Vierendeel beam, that is, the bottom story and top story are in a state of tension-bending and compression-bending, respectively. The axial tension force is continuously transmitted upward, and the models with greater the span-to-depth ratio presented more obvious characteristics of the VA, as illustrated in Fig. 8(a3) and (b3). With the increase in the *L*/*h*, the axial force development of all stories at the initial stage of loading is accelerated, while the change of axial force in the second and third stories during the stage of large-scale deformation continues to decrease with the increase in the *L*/*h*. The axial force of the models RBS-S5 and RBS-D1 exert more effectively, and can finally reach $0.80N_p$ and $0.90N_p$, exhibited obvious characteristics of tension-bending, which indicated that the beam with larger *L*/*h* is more conducive to the axial force development.

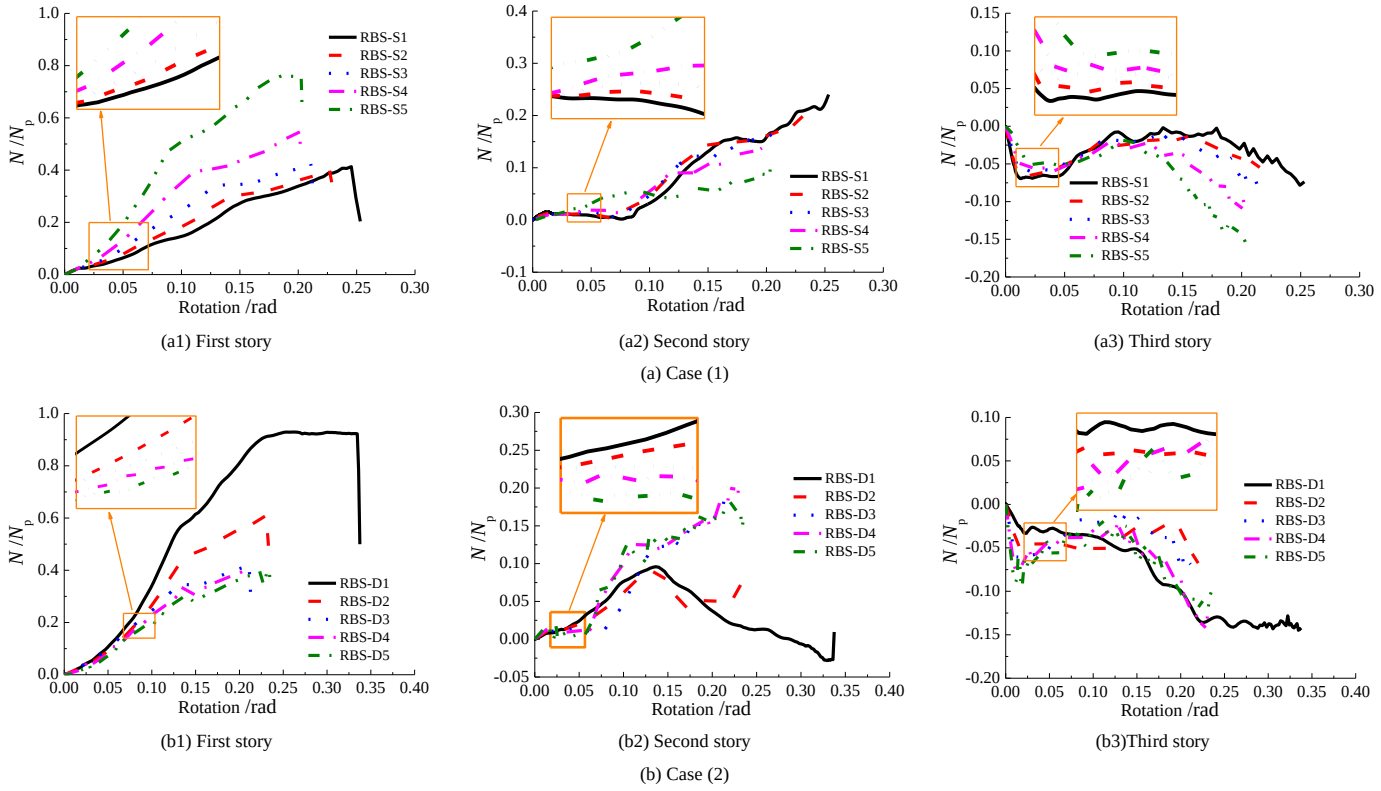

(a1) First story (a2) Second story (a3) Third story

(a) Case (1)

(b1) First story (b2) Second story (b3)Third story

(b) Case (2)

Fig. 8 Comparison of axial force development of models with various span to depth ratios

3.3.2. Bending moment *development*

Fig. 9 compares the normalized bending moment m/m_{pi} at the most unfavorable section of different stories of each model. For the same model, the bending moment of different stories is essentially the same in the initial stage. As the vertical displacement increases, the bending moment of the upper stories decreases continuously, and the higher the number of stories, the greater is the attenuation amplitude. This is mainly because the higher stories in the direct area receive smaller boundary restraint stiffness provided by the peripheral frames. For the different models, the bending moment of models with lager *L*/*h* developed much more quickly. Besides, the development of m_{pi} decreases with the increase of *L*/*h*, and it can be found that the m/m_{pi} of models with a large *L*/*h* does not exceed 1, such as models RBS-S5 and RBS-D1. It shows that the larger *L*/*h* was not conducive to the complete development of the bending capacity of the section and hindered the realization of m_{pi} of the corresponding section.

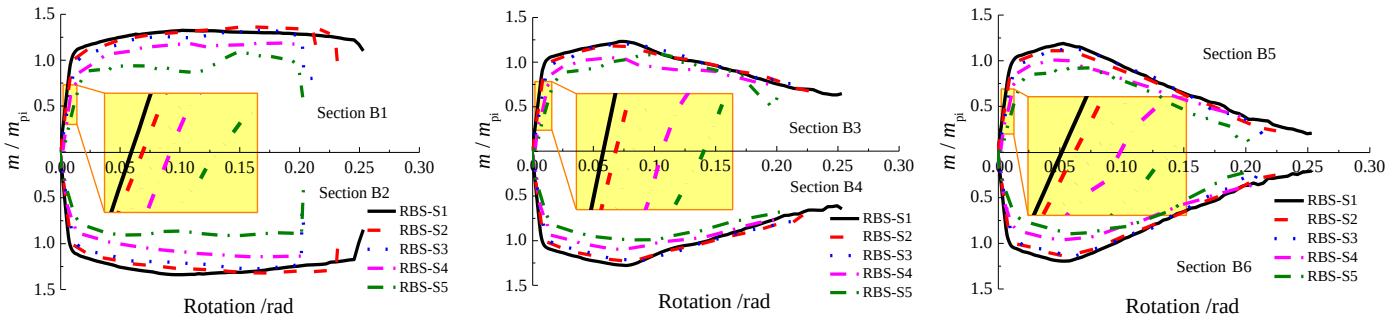

(a1) First story (a2) Second story (a3) Third story

(a) Case (1)

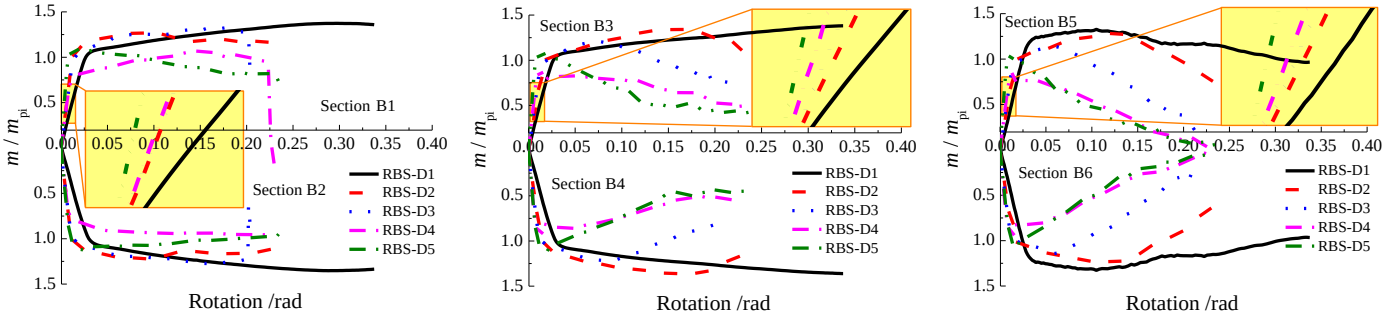

(b1) First story (b2) Second story (b3) Third story

(b) Case (2)

Fig. 9 Comparison of bending moment development of models under different cases

3.4. Overall horizontal deflection

The overall horizontal deflection of models with various span-to-depth ratio is shown in Fig. 10. The horizontal absolute displacement (the horizontal displacement of the side connection of this story relative to the initial position) of side connection at the bottom story of all models is the smallest among each story, while the horizontal relative displacement (the horizontal absolute displacement of the side connection of this story relative to the horizontal absolute displacement of the side connection of the next story) is the largest among each story. On the contrary, the horizontal displacement law of at the top story presented opposite law. Owing to the axial force development of the first story beam has too much demand for peripheral constraints, which leads to the yield of the bottom side column, and causing the peripheral columns of the upper stories can not provide sufficient tie effect for the double-span beams of the corresponding story. On the whole, the horizontal displacement of each story shows the development characteristics of continuous nonlinear decline.

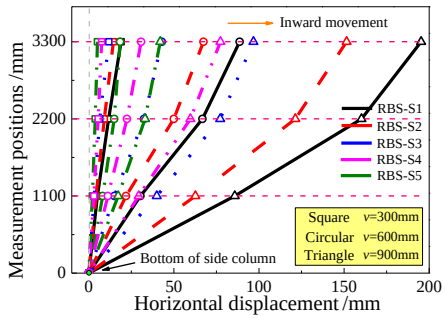

(a) Case (1)

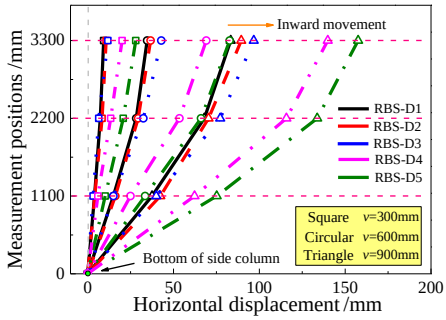

(b) Case (2)

Fig. 10 Comparison of overall horizontal defection of models under different cases

4. Mechanism resistance development and contribution level

The force equilibrium of each story beam of planar steel frame is illustrated in Fig. 11. The catenary mechanism resistance (CMR) and flexural mechanism resistance (FMR) were composed of the axial forces in the beams and shear forces at beam ends, respectively. In general, the resistant contribution of VA to the total resistance was relatively small, which can be classified into FMR [14]. The CMR and FMR can be calculated as stated in Eqs. (14)~(15), and two resistant contribution ratios were introduced to understand the contribution proportion (at one point) of FMR and CMR (μ_F, μ_C) under different vertical loading displacement of failure column. In addition, two resistant contribution coefficients (whole process) of FMR and CMR (α_F, β_C) were proposed based on the energy balance conversion principle [11] to elucidate the contribution proportion of CMR and FMR during entire loading stage, which can be calculated as stated in Eqs. (17)~(18), while α_F is equal to the sum of contribution coefficients of FMR provided by each story (α_{Fi}), and β_C is sum of contribution coefficients of CMR of each story (β_{Ci}). The collapse resistance provided by each story can be calculated according to Eq. (19), and the contribution coefficient of each story (η_i) can be determined in accordance with Eq. (20).

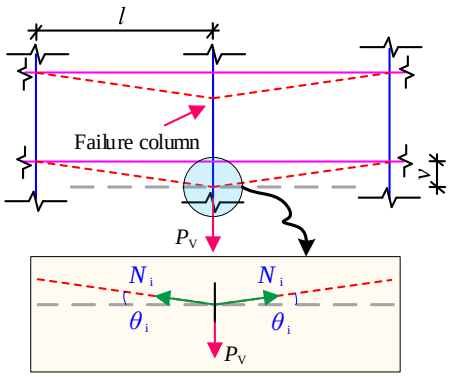

Fig. 11 Force equilibrium of each story beam of planar steel frame

$$P_C = \sum P_{Ci} = \sum (2N_i \sin\theta_i) \tag{14}$$

$$P_F = P_V - P_C \tag{15}$$

$$\mu_F = P_F / P_V,\ \mu_C = P_C / P_V \tag{16}$$

$$\alpha_F = \sum \alpha_{Fi} = \sum \left(\int_0^v P_{Fdi} dv / \int_0^v P_{di} dv\right) \tag{17}$$

$$\beta_C = \sum \beta_{Ci} = \sum \left(\int_0^v P_{Cdi} dv / \int_0^v P_{di} dv\right) \tag{18}$$

$$P_V = N_{C(mx)} = \sum P_i = \sum (N_{C(i+1)} - N_{C(i)}) = \sum (P_{Fi} + P_{Ci}) \tag{19}$$

$$\eta_i = \int_0^v P_{idi} dv / \int_0^v P_{di} dv \tag{20}$$

Here, N_i is the axial force of each story beam; θ_i is the rotation of each story beam end; P_i is the resistance provided by each story; $N_{C(i+1)}$ and $N_{C(i)}$ are the axial forces of the steel columns in the $(i+1)^{th}$ and i^{th} story, respectively; $N_{C(max)}$ is equal to the total resistance; and P_{Fi} and P_{Ci} are the FMR and CMR of each story, respectively.

4.1. Case (1)

The development of the resistance mechanism and related contributions of a multi-story steel frame structure under case (1) are shown in Fig. 12. With the decrease in the *L/h*, the resistance introduced by the catenary and flexural mechanisms increases in turn. As shown in Fig. 12(a) and (b), decreasing the beam span is very conducive to the exertion of catenary action, resulting in the rapid transformation from flexural mechanism to catenary mechanism, as illustrated in Fig. 12(c). However, an excessive small beam span is not conducive to the structural vertical displacement under the removal of the middle column. With the increase in the *L/h*, P_i decreases continuously, as illustrated in Fig. 12(d) ~ (f). However, the contribution coefficients of each story presents opposite results. The resistance coefficient of the first story increases with the increase in the *L/h*, while the resistance coefficient of the second and third stories decreases, as illustrated in Fig. 12(i) and Table 4. The contribution coefficients of CMR and FMR are presented in Fig. 12(g). With the increase in the *L/h*, the contribution of the catenary mechanism continues to increase, and that of the flexural mechanism corresponding to each story decreases in turn.

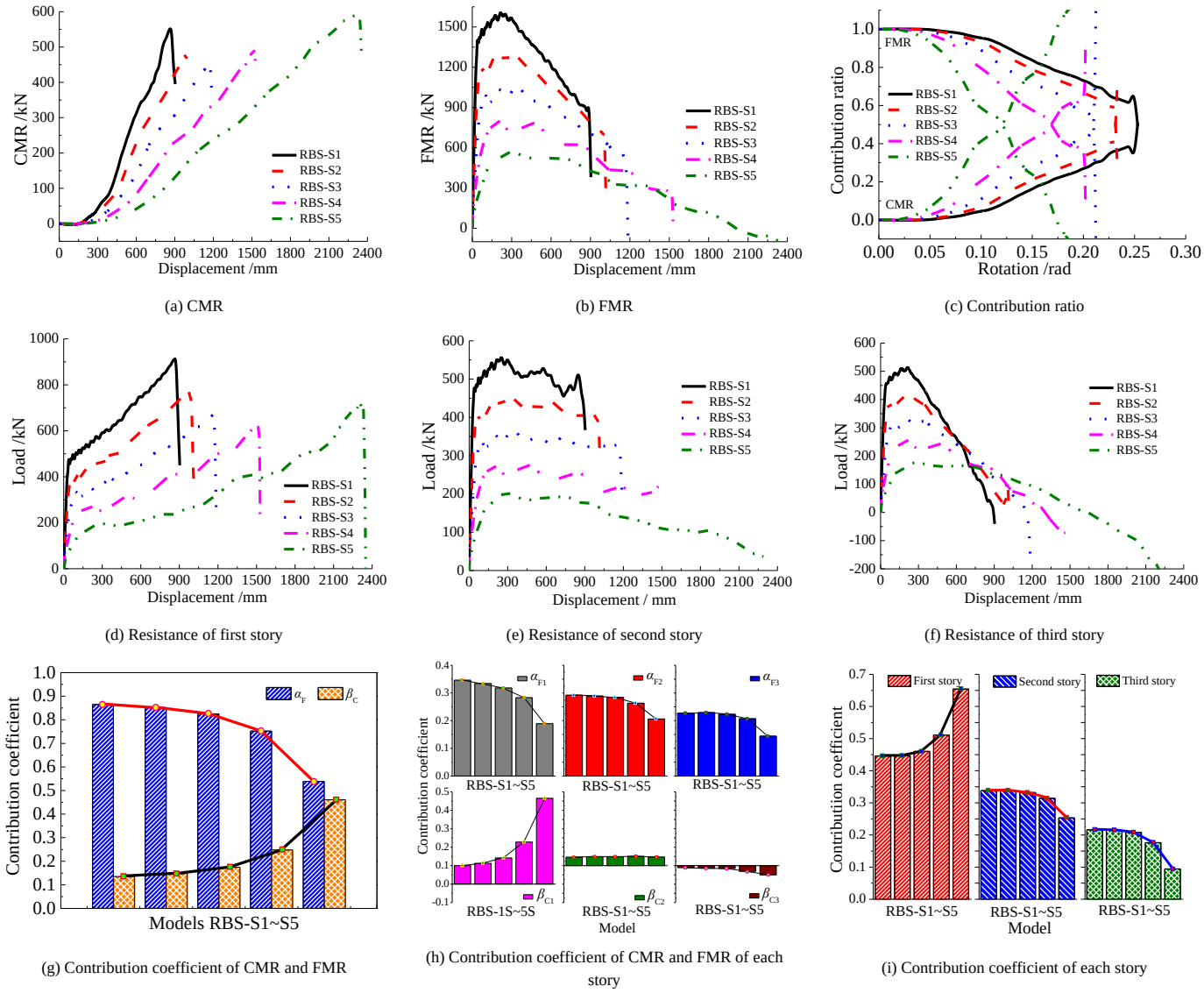

Fig. 12 Resistance development and corresponding contribution coefficients of CMR and FMR of models under case (1)

Table 4
Resistant contribution coefficients of each story beam

Models	α_F	β_C	α_{F1}	α_{F2}	α_{F3}	β_{C1}	β_{C2}	β_{C3}	η_1	η_2	η_3
RBS-S1	0.865	0.135	0.346	0.292	0.227	0.100	0.046	-0.011	0.446	0.338	0.216
RBS-S2	0.852	0.148	0.334	0.289	0.229	0.113	0.049	-0.014	0.447	0.338	0.215
RBS-S3	0.825	0.175	0.318	0.284	0.223	0.142	0.048	-0.015	0.460	0.332	0.208
RBS-S4	0.752	0.248	0.283	0.263	0.207	0.228	0.051	-0.031	0.511	0.314	0.176
RBS-S5	0.539	0.461	0.189	0.206	0.144	0.465	0.047	-0.050	0.654	0.253	0.094

4.2. Case (2)

The development of FMR, CMR and corresponding resistant contribution coefficients of three-story planar steel frames under case (2) are shown in Fig. 13. The development of the CMR of each model was very close, thus, the development trend of FMR provided by each model was completely consistent with that of the load-displacement curve, as illustrated in Fig. 13(a) and (b). The contribution ratios of different mechanism resistances during the entire loading stage is shown in Fig. 13(c). The transformation process from the FMR to CMR of models with a smaller beam depth lags behind other models. The resistance provided by each story with different beam depths is shown in Fig. 13(d)~(f). Fig. 13(g) presents the values of α_F and β_C; it can be seen that with an increase in the beam depth, the α_F decreases, whereas the β_C increases continuously. As illustrated in Fig. 13(h), increasing the beam depth can significant improve the

FMR of the first story (α_{F1}), but it is not conducive to (β_{C1}). The contribution coefficients of each story is summarized in Fig. 13(i) and Table 5. The resistance contribution coefficient of the first story decreases at first and then increases with the increasing beam depth, whereas the resistant contribution coefficient of the second and third stoies first increases and then decreases.

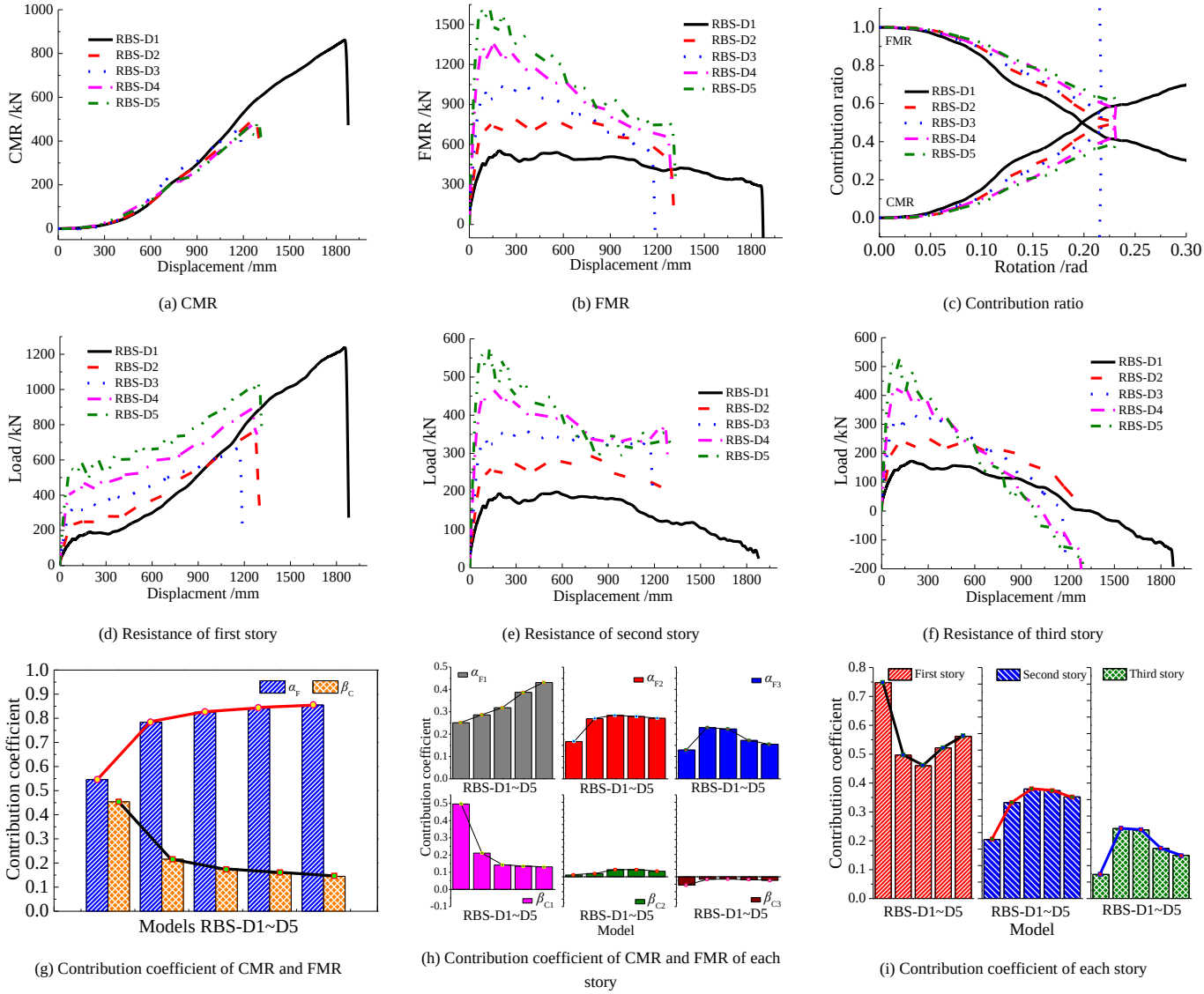

Fig. 13 Resistance development and corresponding contribution coefficients of CMR and FMR of models under case (2)

Table 5
Resistant contribution coefficients of each story beam

Models	α_F	β_C	α_{F1}	α_{F2}	α_{F3}	β_{C1}	β_{C2}	β_{C3}	η_1	η_2	η_3
RBS-D1	0.546	0.454	0.251	0.167	0.129	0.497	0.012	-0.056	0.748	0.179	0.073
RBS-D2	0.784	0.216	0.286	0.269	0.229	0.211	0.022	-0.017	0.497	0.291	0.212
RBS-D3	0.825	0.175	0.318	0.284	0.223	0.142	0.048	-0.015	0.460	0.332	0.208
RBS-D4	0.842	0.158	0.387	0.279	0.172	0.135	0.048	-0.020	0.522	0.327	0.152
RBS-D5	0.855	0.145	0.431	0.271	0.155	0.131	0.037	-0.024	0.562	0.308	0.131

5. Development trend analysis of resistant contribution coefficients

5.1. Contribution coefficients of CMR and FMR

According the resistant contribution coefficients of each story beam (Tables 1 and 2), the 3D surface of contribution coefficients of FMR and FMR under cases (1) and (2) can be nonlinear fitted, as presented in Fig. 14. The value of α_F increase with the decrease of *L*/*h*. The resistance contribution coefficients of CMR exhibited the opposite law. According to the contribution coefficients of CMR and FMR under cases (1) and (2), the empirical formulas for CMR and FMR of double-span beams under cases (1) and (2) were proposed, as illustrated in Eqs. (21) and (22).

$$\beta_C = 0.958 - 3.280\times h - 2.484\times10^{-2}L + 3.123h^2 + 3.672\times10^{-3}L^2 - 1.838\times10^{-2}hL, \quad R^2 = 0.929 \tag{21}$$

$$\alpha_F = 1-\beta_C = 0.043 + 3.280\times h + 2.484\times10^{-2}L - 3.123h^2, \quad R^2 = 0.929 + 3.672\times10^{-3}L^2 - 1.838\times10^{-2}hL \tag{22}$$

R^2 is fitting coefficient, the units of beam span and beam depth were m.

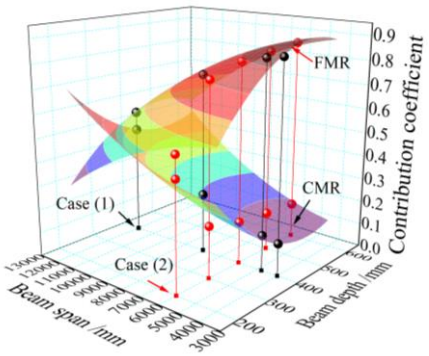

Fig. 14 Contribution coefficient of different mechanism resistances under cases (1)~(2)

5.2. Contribution coefficients of each story

The fitting 3D surface of contribution coefficients of each story under cases (1) and (2) is illustrated in Fig. 15, and the empirical formulas for the contribution coefficients of each story to the total resistance of models with various span-to-depth ratios were proposed, as illustrated in Eqs. (23)~(25), which can be provide a basic and reference for collapse resistance evaluation before the anti-progressive collapse design of multi-story planar steel frames with various span-to-depth ratios.

$$\eta_1 = 1.103 - 0.004\times h - 2.795\times10^{-2}L + 4.797h^2 + 2.734\times10^{-3}L^2 - 1.128\times10^{-1}hL, \quad R^2 = 0.937 \tag{23}$$

$$\eta_2 = 0.135 - 0.136\times h - 3.860\times10^{-2}L - 2.202h^2 - 1.175\times10^{-3}L^2 + 1.166\times10^{-1}hL, \quad R^2 = 0.986 \tag{24}$$

$$\eta_3 = 1-\eta_1-\eta_2 = -0.236 - 1.031\times10^{-2}h - 2.590\times10^{-3}L - 1.574\times10^{-3}h^2 - 1.574\times10^{-3}L^2 - 2.003\times10^{-3}hL, \quad R^2 = 0.876 \tag{25}$$

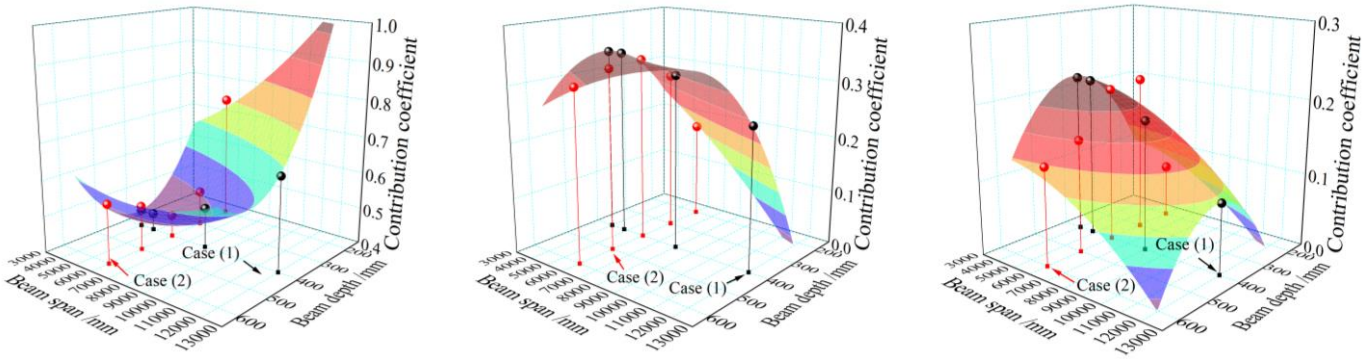

(a) First story (b) Second story (c) Third story

Fig. 15 Resistant contribution coefficient of each story under cases (1)~(2)

6. Conclusion

In this study, the three-story planar steel frames were employed to study the effect of the span-to-depth ratio of double-span beams on the structural collapse performance through the refined numerical modeling method, and makes a more comprehensive analysis on the collapse resistance level, internal force development, deformation characteristics, loading-resisting mechanisms and corresponding resistant contribution coefficients, The following conclusions are obtained:

(1) The effect of VA on the internal force development of each story beam is reflected considering the following two aspects: One hand, VA reflects the lag effect of the axial force transmission across each story, and the axial tension is continuously transmitted upward with as the increasing of structural displacement. On the other hand, VA increases the attenuation degree of bending moment among the stories from bottom to top. A combination of the above two factors leads to the largest contribution of resistance provided by the bottom story, followed by the upper story, and the lowest resistance contributed by the top story. The essence of this phenomenon is that the tie effect of the peripheral frames on the sub-fame decreases from bottom to top.

(2) The FMR and CMR were distributed by the span-to-depth ratio and beam span, respectively. Although decreasing span-to-depth ratio has a beneficial effect on the improvement of structural collapse resistance, but it was also adverse to the vertical displacement development under column removal scenario.

(3) The contribution coefficient of FMR decreases with the increasing span-to-depth ratio, whereas the contribution coefficient of CMR exhibits the opposite development law. Increasing the beam span increases the resistance contribution of the bottom story and decreases the resistance contribution coefficients of the upper stories. With a continuously increasing beam depth, the resistance contribution coefficient of the bottom stories increases at first and then decreases, while the upper stories exhibit an opposite trend.

(4) The theoretical formulas of collapse-resistant capacity were empirical proposed through nonlinear fitting the contribution coefficients of different resistance mechanisms of each story, which can provide a more important reference for collapse resistance evaluation before the design of multi-story steel frames to resist progressive collapse.

Acknowledgments

The works in this paper was sponsored by the National Natural Science Foundation of China [grant numbers 51678476, 51908449], Scientific research plan projects of Shaanxi Education Department [grant number 20JY033, 20JK0713].

References

[1] Meng B., Li L.D., Zhong W.H., et al., “Improving anti-progressive collapse capacity of welded connection based on energy dissipation cover-plates”, Journal of Constructional Steel Research, 188:107051, 2022.
[2] DOD. Design of buildings to resist progressive collapse: UFC 4-023-03 [S]. Washington, D. C.: Department of Defense, 2009.
[3] Dinu F., Marginean I., Dubina D., “Experimental testing and numerical modelling of steel moment-frame connections under column loss”, Engineering Structures, 151: 861–878, 2017.
[4] Zhong W.H., Tan Z., Meng B., et al. “Comparative evaluation of collapse behavior at different structural levels with different connections”, Journal of Constructional Steel Research, 193: 107280, 2022.
[5] Yang B., Tan K.H., “Experimental tests of different types of bolted steel beam-column joints under a central-column-removal scenario”, Engineering Structures, 54: 112–130, 2013.
[6] Tan Z., Zhong W.H., Meng B., et al., “Effect of various boundary constraints on the collapse behavior of multi-story composite frames ”, Journal of Building Engineering, 52: 104412, 2022.
[7] Weng J., Lee C.K., Tan K.H., et al., “Damage assessment for reinforced concrete frames subject to progressive collapse”, Engineering Structures, 149: 147–160, 2017.
[8] Tan Z., Zhong W.H., Tian L.M., et al., “Research on the collapse-resistant performance of composite beam–column substructures using multi-scale models”, Structures, 27: 86–101, 2020.
[9] Zhong W.H., Tan Z., Song X.Y., et al., “Anti-collapse analysis of unequal span steel beam-column substructure considering the composite effect of floor slabs”, Advance Steel Construction, 15(4): 377–385, 2019.

[10] Zhong W.H., Tan Z., Tian L.M., et al., “Collapse resistance of composite beam-column assemblies with unequal spans under an internal column-removal scenario”, Engineering Structures, 206: 110143, 2020.
[11] Tan Z., Zhong W.H., Tian L.M., et al., “Quantitative assessment of resistant contributions of two-bay beams with unequal spans”, Engineering Structures, 242: 112445, 2021.
[12] Zhang W.J., Li G.Q., Zhang J.Z., “Progressive collapse mechanism of steel frames-structures subjected to a middle-column loss”, Advanced Steel Construction, 17(2):199–209, 2021.
[13] Meng B., Hao J.P., Zhong W.H., “Numerical study on the anti-progressive collapse performance of steel frame-steel plate shear wall structures,” Journal of Building Engineering, 35: 102049, 2021.
[14] Meng B., Li L.D., Zhong W.H., et al., “Enhancing collapse-resistance of steel frame joints based on folded axillary plates”, Advanced Steel Construction, 17(1): 84–94, 2021.
[15] Gao S., Xu M., Guo L.H., et al., “Behavior of CFST-column to steel-beam joints in the scenario of column loss”, Advanced Steel Construction, 15(1): 47–54: 2019.
[16] Li G.Q., Zhang J.Z., Li L.L., et al., “Progressive collapse resistance of steel framed building under extreme events”, Advanced Steel Construction, 17(3): 318–330, 2021.
[17] Sasani M., Bazan M., Sagiroglu S., “Experimental and analytical progressive collapse evaluation of actual reinforced concrete structure”, ACI Structural Journal, 104(6): 731–739, 2007.
[18] Li G.Q., Zhang J.Z., Jiang J., “Multi-story composite framed-structures due to edge-column loss”, Advanced Steel Construction, 16(1): 20–29, 2020.
[19] Qian K., Lan X., Li Z., et al., “Progressive collapse resistance of two-storey seismic configured steel sub-frames using welded connections”, Journal of Constructional Steel Research, 170: 106117, 2020.
[20] Qian K., Lan X., Li Z., et al., “Behavior of steel moment frames using top-and-seat angle connections under various column-removal scenarios”, Journal of Structural Engineering, 147(10): 04021144, 2021.
[21] Tsitos A., Mosqueda G., Filiatrault A., et al., “Experimental investigation of progressive collapse of steel frames under multi-hazard extreme loading”, In The 14th World Conference on Earthquake Engineering, Beijing, China, 2008.
[22] Zhong W.H., Tan Z., Song X.Y., et al., “Collapse-resistant performance of a single-story frame assembly and multi-story sub-frame under an internal column-removal scenario”, Steel and Composite Structures, 41(5): 663-679, 2021.
[23] Tan Z., Zhong W.H., Tian L.M., et al., “Numerical study on collapse-resistant performance of multi-story composite frames under a column removal scenario”, Journal of building Engineering, 44: 102957, 2021.
[24] Yi W.J., He Q.F., Xiao Y., et al., “Experimental study on progressive collapse-resistant behavior of reinforced concrete frame structures”, ACI Structural Journal, 105(4): 433–439, 2008.
[25] Ahmadi E., Hosseini S.A., “Capacity evaluation of eight bolt extended endplate moment connections subjected to column removal scenario”, Advanced Steel Construction, 17(3): 273–282, 2021.
[26] Li H.H., Zhang B.Y. Cai X.H., “Assessment of design requirements against progressive collapse in UFC 4-023-03: numerical simulation”, Advanced Steel Construction, 14(4): 514–538, 2018.
[27] Tan Z., Zhong W.H., Duan S.C., et al., “Research on anti-collapse performance of composite beam-column substructures with different beam line stiffness”, Journal of Vibration and Shock, 40(10): 57–66, 2021.
[28] GB 50017-2017. Standard for design of steel structures, China Architecture & Building Press, Beijing, China, 2017.
[29] Tan Z., Zhong W.H., Meng B., et al., “Numerical evaluation on collapse-resistant performance of steel-braced concentric frames ”, Journal of Constructional Steel Research, 193: 107268, 2022.
[30] ANSI/AISC 358-10. Prequalified Connections for Special and Intermediate Steel Moment Frames for Seismic Applications, AISC; 2014.
[31] ABAQUS. Abaqus Analysis User’s Guide (6.14), ABAQUS Inc.; 2014.
[32] Yu H.L., Jeong D.Y., “Application of a stress triaxiality dependent fracture criterion in the finite element analysis of unnotched Charpy specimens”, Theoretical and Applied Fracture Mechanics, 54(1): 54–62, 2010.
[33] Izzuddin B.A., Vlassis A.G., Elghazouli A.Y., et al., “Progressive collapse of multi-storey buildings due to sudden column loss – Part I: Simplified assessment framework”, Engineering Structures, 30(5): 1308–1318, 2008.